Available online at www.sciencedirect.com
SCIENCE DIRECT
Journal of Nuclear Materials 351 (2006) 88–99
journal of nuclear materials
www.elsevier.com/locate/jnucmat

Solute interaction with point defects in α Fe during thermal ageing: A combined ab initio and atomic kinetic Monte Carlo approach

E. Vincent [a,b,*], C.S. Becquart [a], C. Domain [a,b]

[a] *Laboratoire de Métallurgie Physique et Génie des Matériaux, UMR8517, Université de Lille 1, F-59655 Villeneuve d'Ascq cédex, France*
[b] *Electricité de France-R&D, Département Matériaux et Mécanique des Composants, Les Renardières, F-77818 Moret sur Loing cédex, France*

Abstract

Solute Cu plays a major role in the embrittlement of reactor pressure vessel (RPV) steels under radiation. In RPV steels and dilute FeCu alloys, characterization techniques such as the tomographic atom probe (TAP), or the small angle neutron scattering (SANS) have revealed the formation of solute rich clusters (with Cu, Ni, Mn and Si) under neutron flux. It is thus very important to characterize the interactions of these solutes with radiation-induced point defects in order to understand the elementary mechanisms behind the formation of these clusters. Ab initio calculations based on the density functional theory have been made in order to build a database used to parameterise an atomic kinetic Monte Carlo model. The interactions of point defects and solute atoms in dilute FeX alloys (X = Cu, Mn, Ni or Si) have been evaluated for different configurations of small solute clusters and solute–vacancy complexes. First results obtained with the kinetic Monte Carlo model will be presented and compared to some experimental observations.

PACS: 61.72.Ji; 61.80.−x; 71.20.Be; 71.15.Mb

1. Introduction

In light water reactors, neutron irradiation is responsible of the embrittlement of the pressure vessel steels. The characterization techniques have revealed that the hardening of the steels is concurrent with the formation of neutron radiation-induced clusters, enriched in Cu, Ni, Mn and Si solute atoms. But the composition of these clusters is still a debate [1]. Indeed, with small angle neutron scattering and field emission scanning transmission electron microscopy, these clusters are similar to precipitates [2,3] whereas with the tomographic atom probe, they appear to be more or less dilute clusters sometimes called atmospheres [4–7]. Whatever the Fe content of these nanometer size clusters, since in in-service pressure vessel steels, and at the in-service temperature, the ferrite matrix is undersaturated with Ni, Si and Mn, it is surprising to observe these elements within the clusters.

* Corresponding author. Address: Electricité de France-R&D, Département Matériaux et Mécanique des Composants, Les Renardières, F-77818 Moret sur Loing cédex, France.
E-mail address: edwige.vincent@edf.fr (E. Vincent).

0022-3115/$ - see front matter
doi:10.1016/j.jnucmat.2006.02.018

The modelling of the formation of these solute rich clusters has up to now been based on thermodynamics or Metropolis Monte Carlo [8,9]. In this previous work, simple pair interactions have been derived from mixing energies of the various binary alloys. For some of the binary systems, the mixing energies had to be estimated (e.g. for the bcc CuNi system which is not stable and for which no thermodynamical data were available). These simulations have provided the equilibrium composition of the solute rich clusters, however, they did not bring any information about the kinetics and the time required for their formation. Recently, a simple dynamical Ising model also based on thermodynamical data has been built and used to simulate the annealing of a FeCuNiMnSi alloy [10].

Consequently, the simulation of the formation of these clusters in the host Fe matrix requires a better knowledge of the energetic properties of these elements in bcc Fe as well as of their migration energies in order to obtain information on the kinetic. These elementary properties at the atomic level are most of the time not known experimentally and can be obtained by ab initio calculations. Thus, ab initio calculations have been made [11] to investigate the kind of interaction which exists between the point defects created by the displacement cascades and the Cu, Ni, Mn and Si solute atoms. This knowledge is essential to study the long term evolution of the microstructure in pressure vessel steels under irradiation. These ab initio data are now used in an atomic kinetic Monte Carlo (AKMC) code to model the microstructural evolution of a dilute Fe–CuNiMnSi complex alloy.

In a first part, the Monte Carlo method is described as well as the parameterisation scheme to describe the interactions. Then, in a second part, the first results are presented and compared to some experimental observations.

2. Methodology

2.1. Ab initio calculations

Our calculations have been done using the Vienna Ab initio Simulation Package VASP [12,13]. They were performed in a plane-wave basis, using fully nonlocal Vanderbilt-type ultrasoft pseudopotentials to describe the electron–ion interaction. Exchange and correlation were described by the Perdew–Zunger functional, adding a non-local correction in the form of the generalised gradient approximation (GGA) of Perdew and Wang. All the calculations were done in the spin polarised GGA using the supercell approach with periodic boundary conditions. The ultrasoft pseudopotentials used in this work come from the VASP library. Brillouin zone (BZ) sampling was performed using the Monkhorst–Pack scheme. The defect calculations were done at constant volume thus relaxing only the atomic position in a supercell dimensioned with the equilibrium lattice parameter for Fe (2.8544 Å). The plane wave cut-off energy was 240 eV. The calculation convergence with the supercell size has been previously examined [11,14] and was found to be achieved most of the time for 54-atom supercells sampled by 125 k points (especially when no interstitial was considered). As a consequence, the results presented here are those obtained either using 54-atom supercells with a BZ sampling of 125 k points or 128-atom supercells with 27 k points. More details on the method and, in particular, a comparison of full relaxation versus constant volume calculations for defects in Fe can be found in a previous work [14].

The binding energy between two entities, A and B, in a bcc iron matrix containing N atomic sites, is calculated as follows:

$$E_b(A,B) = [E(N-1+A) + E(N-1+B)] - [E(N-2+A+B) + E_{ref}], \quad (1)$$

where $E(N-1+A)$ is the energy of a supercell containing only defect A, $E(N-1+B)$ the energy of the same supercell containing only defect B, $E(N-2+A+B)$ the energy of the same supercell containing A and B and E_{ref} the energy of the supercell containing no defect.

In this scheme, a positive binding energy indicates an attractive interaction.

The solution enthalpy, corresponding to an infinite dissolution, is determined as follows:

$$E_{mix}(X => \mathrm{Fe}) = [E((N-1)\mathrm{Fe}+A)_{bcc} - ((N-1)/N)E_{ref} - E(A_{ref})], \quad (2)$$

where $E((N-1)\mathrm{Fe}+A)_{bcc}$ is the energy of a supercell containing $(N-1)$Fe atoms and one solute atom A, E_{ref} is the energy of a supercell containing N Fe atoms and $E(A_{ref})$ is the cohesive energy of solute A in the reference state chosen.

2.2. Atomic kinetic Monte Carlo method

Our simulations have been made using the LAKIMOCA code developed at EDF [15]. This code initially developed for FeCu has been adapted to treat more complex alloys with substitutional elements such as Cu, Ni, Mn and Si solute atoms in a rigid α-Fe matrix. The code relies on the residence time algorithm derived by Young and Elcock [16] to model the diffusion of a vacancy in FeCu. The basic assumption in this model is that the vacancy diffuses via a series of first nearest neighbour jumps. Each jump is thermally activated and its frequency is given by

$$\Gamma_{\mathrm{X,V}} = \nu_{\mathrm{X}} \exp\left(-\frac{E_{\mathrm{a}}}{kT}\right). \tag{3}$$

ν_{X} is the attempt frequency for the entity X (X = Fe, Cu, Ni, Mn or Si) which makes an exchange with the vacancy and E_{a} is the activation energy of the jump. The attempt frequencies ν_{X} are all taken equal to $6 \times 10^{12}\ \mathrm{s}^{-1}$. For each step, the probabilities (given by $\Gamma_{\mathrm{X,V}}$) of all the 8 possible jumps of all the vacancies are determined (the probability of two vacancies switching sites was set to zero). Then, for each vacancy, a jump is chosen at random with a weight corresponding to its probability and the mean residence time corresponding to the chosen transition is calculated. This time is given by the inverse of the sum of all the frequencies $\Gamma_{\mathrm{X,V}}$. The activation energy (or migration barrier) is one of the most important parameter of the model and many ways of determining it have been proposed [9,17–19]. As a compromise must be done between the computer calculation time and the precision of the results, a simple but environment-dependent form for E_{a}, which satisfies the detailed balance rule, has been chosen. It is given by

$$E_{\mathrm{a}} = E_{\mathrm{a}_0} + \frac{E_{\mathrm{f}} - E_{\mathrm{i}}}{2}. \tag{4}$$

E_{a_0} depends only on the type of the migrating atom: it is the vacancy migration energy in pure Fe (0.65 eV [14]) when the vacancy jumps towards a Fe atom and it is the solute migration energy when the vacancy jumps towards a solute atom. These energetic barriers were determined by ab initio calculations using 54 atom supercells (Table 1). E_{i} and E_{f} are the potential energies of the system before and after the vacancy jump, respectively. The activation energy of the jump can also be obtained using different models: empirical interatomic potentials [19], pair interaction models with 'broken' bond model [17,18,20,21]. Because of the number of different solute atoms and the lack of interatomic potentials, we have chosen to calculate the activation energy, and thus the potential energies of the system (E_{i} and E_{f}) using pair interactions. Since the interactions are non-negligible in second nearest neighbour positions, the chemical interactions between all the entities which compose the system have been described by first and second neighbour pair interactions, according to the following equation:

Table 1
Migration energies (eV) in a bcc iron matrix determined by ab initio calculations using supercells of 54 atoms and 125 k points

	Cu	Ni	Mn	Si	Fe
$E_{\mathrm{mig}}(\mathrm{X}^{\mathrm{Fe}})$	0.56	0.70	1.03	0.44	0.65

$$E = \sum_j \varepsilon^{(i)}_{(\mathrm{Fe\text{–}Fe})} + \sum_k \varepsilon^{(i)}_{(\mathrm{V\text{–}V})} + \sum_l \varepsilon^{(i)}_{(\mathrm{Fe\text{–}V})} + \sum_m \varepsilon^{(i)}_{(\mathrm{Fe\text{–}X})} + \sum_n \varepsilon^{(i)}_{(\mathrm{V\text{–}X})} + \sum_p \varepsilon^{(i)}_{(\mathrm{X\text{–}Y})}, \tag{5}$$

where i equals 1 or 2 and corresponds respectively to first or second nearest neighbour interaction, j is the number of Fe–Fe bonds, k the number of V–V bonds, l the number of Fe–V bonds, m the number of Fe–X (X = Cu, Ni, Mn and Si) bonds, n the number of V–X bonds and p the number of X–Y (X and Y = Cu, Ni, Mn and Si) bonds of the lattice.

2.2.1. Parameterisation of the atomic interactions

The pair interactions which have to be determined to describe the alloy of interest must take into account vacancies, iron and solute atoms. We have chosen to adjust them to ab initio calculations by expressing several properties as functions of these pair interactions.

For a binary alloy, in our case Fe–X (X = Cu, Ni, Mn or Si), twelve pair interactions, and consequently twelve relations, are required. The binding energies (E_{b}) between two vacancies, two solute atoms (X) and between a vacancy and a solute X have been used. They are given by

$$E^{(i)}_{\mathrm{b(X\text{–}X)}} = 2\varepsilon^{(i)}_{(\mathrm{Fe\text{–}X})} - \varepsilon^{(i)}_{(\mathrm{Fe\text{–}Fe})} - \varepsilon^{(i)}_{(\mathrm{X\text{–}X})}, \tag{6}$$

$$E^{(i)}_{\mathrm{b(V\text{–}V)}} = 2\varepsilon^{(i)}_{(\mathrm{Fe\text{–}V})} - \varepsilon^{(i)}_{(\mathrm{Fe\text{–}Fe})} - \varepsilon^{(i)}_{(\mathrm{V\text{–}V})}, \tag{7}$$

$$E^{(i)}_{\mathrm{b(V\text{–}X)}} = \varepsilon^{(i)}_{(\mathrm{Fe\text{–}X})} + \varepsilon^{(i)}_{(\mathrm{Fe\text{–}V})} - \varepsilon^{(i)}_{(\mathrm{Fe\text{–}Fe})} - \varepsilon^{(i)}_{(\mathrm{V\text{–}X})}, \tag{8}$$

i equals 1 or 2 and stands for first or second nearest neighbour, respectively. Moreover, the pair interactions between two Fe atoms $\left(\varepsilon^{(i)}_{(\text{Fe–Fe})}, i \in \{1,2\}\right)$ or two solute atoms X $\left(\varepsilon^{(i)}_{(\text{X–X})}, i \in \{1,2\}\right)$ are related to the cohesive energies of the corresponding pure metals by

$$E_{\text{coh}}(\text{Fe}) = 4\varepsilon^{(1)}_{(\text{Fe–Fe})} + 3\varepsilon^{(2)}_{(\text{Fe–Fe})}, \tag{9}$$

$$E_{\text{coh}}(\text{X}) = 4\varepsilon^{(1)}_{(\text{X–X})} + 3\varepsilon^{(2)}_{(\text{X–X})}. \tag{10}$$

For all solutes, the cohesive energies considered in Eq. (10) are those obtained for the bcc structure as the Fe matrix is bcc and the clusters are very diluted or the precipitates small and coherent with the matrix. The vacancy formation energy in a pure Fe lattice has also been used, and leads to the following equation:

$$E_{\text{for}}(\text{V}^{\text{Fe}}) = 8\varepsilon^{(1)}_{(\text{Fe–V})} + 6\varepsilon^{(2)}_{(\text{Fe–V})} - 4\varepsilon^{(1)}_{(\text{Fe–Fe})} - 3\varepsilon^{(2)}_{(\text{Fe–Fe})}. \tag{11}$$

With the knowledge of $E^{(i)}_{\text{b(X–X)}}, E^{(i)}_{\text{b(V–V)}}, E^{(i)}_{\text{b(V–X)}}$ $i \in \{1,2\}$, $E_{\text{coh}}(\text{Fe})$, $E_{\text{coh}}(\text{X})$ and $E_{\text{for}}(\text{V}^{\text{Fe}})$, all the pair interactions can be calculated except $\varepsilon^{(2)}_{(\text{Fe–Fe})}, \varepsilon^{(2)}_{(\text{Fe–V})}$ and $\varepsilon^{(2)}_{(\text{X–X})}$. We have chosen to correlate the later with a simple relation, to those obtained by the set of Eqs. (6)–(11), by

$$\varepsilon^{(2)}_{(\text{Fe–Fe})} = \alpha\varepsilon^{(1)}_{(\text{Fe–Fe})} \tag{12}$$

$$\varepsilon^{(2)}_{(\text{Fe–V})} = \beta\varepsilon^{(1)}_{(\text{Fe–V})} \tag{13}$$

$$\varepsilon^{(2)}_{(\text{X–X})} = \lambda_{\text{X}}\varepsilon^{(2)}_{(\text{Fe–Fe})} \tag{14}$$

α and β are constants and λ_{X} is a solute depending constant.

To treat more complex alloys, the equations above including solute atoms, i.e. Eqs. (6), (8), (10) and (14) have to be included for the new solute atoms, as well as the crossed solute binding energies which are given by

$$E^{(i)}_{\text{b(X–Y)}} = \varepsilon^{(i)}_{(\text{Fe–X})} + \varepsilon^{(i)}_{(\text{Fe–Y})} - \varepsilon^{(i)}_{(\text{Fe–Fe})} - \varepsilon^{(i)}_{(\text{X–Y})}, \tag{15}$$

X, Y are two different solute atoms and i equals 1 or 2 for first or second nearest neighbour interaction.

The binding and the formation energies used above have been determined by ab initio calculations with 128 atom supercells and 27 k points and are gathered in Tables 2 and 3. The convergence with the supercell size was checked [15]. These ab initio data are globally in agreement with the experimental data.

The binding energies between two similar solute atoms (Table 2) are coherent with the solution enthalpies in bcc Fe we had determined in a previous work [11] and the experimental binary phase diagrams, except for Mn: the two Mn–Mn binding energies are too negative from what could be

Table 2
Solute–solute binding energies (eV) in first (1nn) and second (2nn) nearest neighbour used to calculate the pair interactions for a Fe–CuNiMnSi system

	Cu	Ni	Mn	Si
E_{b}(Cu–X 1nn)	0.14	0.04	0.04	0.05
E_{b}(Cu–X 2nn)	0.03	−0.01	−0.07	−0.05
E_{b}(Ni–X 1nn)		−0.07	−0.06	0.03
E_{b}(Ni–X 2nn)		−0.02	−0.11	−0.11
E_{b}(Mn–X 1nn)			−0.28	0.01
E_{b}(Mn–X 2nn)			−0.15	−0.33
E_{b}(Si–X 1nn)				−0.31
E_{b}(Si–X 2nn)				−0.16

These energies were determined by ab initio calculations with 128 atom supercells and 27 k points. The Mn always stabilises in an antiferro-magnetic state.

Table 3
Vacancy–solute binding energies (eV) calculated by ab initio calculations with 128 atom supercells and 27 k points and used to determine the pair interactions for a Fe–CuNiMnSi alloy

	Cu	Ni	Mn	Si	Vacancy	Fe
E_{b}(V–X 1nn)	0.17	0.03	0.12	0.24	0.14	
E_{b}(V–X 2nn)	0.19	0.18	0.07	0.14	0.28	
E_{b}(V–X)	0.11 [35]	0.21 [35]	0.15 [36]	0.21 [35]		
Exp.	0.14 [36]	0.22 [36]		0.23 [36]		
$E_{\text{for}}(\text{V}^{\text{Fe}})$					2.02	
$E_{\text{for}}(\text{V}^{\text{Fe}})$ Exp.					1.53 [37]–2 [38]	
E_{coh}(X)	−3.49	−4.34	−2.92	−4.03		−4.28 [30]

For the Mn, the state is antiferro-magnetic. The ab initio results are compared with the available experimental data. The vacancy formation energy in an α-Fe matrix is also an ab initio result. See text for more details on the calculations of the cohesive energies for the bcc structures.

expected of the almost ideal character of the Fe–Mn solution.

The solute–solute binding energies, for two different solutes, are also globally in agreement with the experimental ternary phase diagrams Fe–X–Y (X, Y = Cu, Ni, Mn, Si). For the Cu–Fe–Si and the Cu–Fe–Mn ternary systems, they are consistent with the tie-lines determined in the isothermal sections of the ternary systems [22,23]. For the Fe–Ni–Si system they are in agreement with the sign of the experimental interaction parameters determined in liquid iron-base alloys [24,25]. They are also in agreement with the activity coefficients calculated for Ni in the Cu–Fe–Ni system and for Mn in the Fe–Mn–Si system [26,27]. Some discrepancies exist with the Mn–Ni [24,28] and the Mn–Si [24] interactions. Indeed, Mn is a difficult element to model certainly because of its high complexity from the point of view of its magnetic properties. Mn stabilises in a complex crystal structure containing 58 atoms in a cubic unit cell with magnetically non-equivalent atomic sites. Different experimental investigations seem to indicate that this structure exhibits a noncollinear antiferromagnetic structure [29]. In our simulations, all the solutes, and thus Mn are treated using collinear spins. This can be the reason for the problems encountered with this element in our calculations. Therefore, we have started to investigate the influence of the noncollinearity of the spins.

The binding energies with the vacancy (Table 3) agree with the experimental data available and the vacancy formation energy in pure bcc Fe agrees also with the upper boundary of the available experimental data. A detailed comparison appears in [11].

As the absolute energies obtained with the VASP code (and in many other ab initio codes) have usually to be rescaled to be comparable to, for instance, experimental cohesive energies, the solute cohesive energies for the bcc structures in Table 3 have been obtained for each solute by determining by ab initio calculations the difference in energy between the most stable phase and the bcc phase and by adding this energy difference to the experimental cohesive energy [30].

In order to insure that the binding energies and the cohesive energies used to solve Eqs. (6)–(15) are correct and well adapted to the study, other energies, more precisely, interface energies, mixing energies, migration energies (other than the solute migration energies which are presented in Table 1) and vacancy formation energies in bcc solute metals, that were not used in the parameterisation, have been calculated and compared to the ab initio results. Indeed all these energies can be expressed in terms of the properties used in the parameterisation of the cohesive model, as follows:

$$E_{\mathrm{int}}(1\,0\,0) = 2E^{(1)}_{\mathrm{b(X\text{–}X)}} + E^{(2)}_{\mathrm{b(X\text{–}X)}}, \tag{16}$$

$$E_{\mathrm{int}}(1\,1\,0) = 2E^{(1)}_{\mathrm{b(X\text{–}X)}} + 2E^{(2)}_{\mathrm{b(X\text{–}X)}}, \tag{17}$$

$$E_{\mathrm{mix}}(\mathrm{X} \Rightarrow \mathrm{Fe}) = 4E^{(1)}_{\mathrm{b(X\text{–}X)}} + 3E^{(2)}_{\mathrm{b(X\text{–}X)}}, \tag{18}$$

$$E_{\mathrm{mig}}(\mathrm{Fe},\ \mathrm{X}\ 2\mathrm{nn}) = E_{\mathrm{mig}}(\mathrm{V}^{\mathrm{Fe}}) + \frac{E^{(1)}_{\mathrm{b(V\text{–}X)}} - E^{(2)}_{\mathrm{b(V\text{–}X)}}}{2}, \tag{19}$$

$$E_{\mathrm{mig}}(\mathrm{Fe},\ \mathrm{X}\{3|5\}\mathrm{nn}) = E_{\mathrm{mig}}(\mathrm{V}^{\mathrm{Fe}}) + \frac{E^{(1)}_{\mathrm{b(V\text{–}X)}} - E^{(\{3|5\})}_{\mathrm{b(V\text{–}X)}}}{2} \equiv E_{\mathrm{mig}}(\mathrm{V}^{\mathrm{Fe}}) + \frac{E^{(1)}_{\mathrm{b(V\text{–}X)}}}{2}, \tag{20}$$

as we consider only first and second nearest neighbour interactions. The three migration energies above (Eqs. (19) and (20)) are illustrated in Fig. 1 and correspond to the migration of an iron atom towards a vacancy when a solute atom X is situated in a second, third or fifth nearest neighbour position to the migrating atom. The ab initio (1 0 0) and (1 1 0) interface energies were calculated respectively using a 10 and a 16-atom supercell with $10 \times 10 \times 1$ and $10 \times 8 \times 1$ k points and the Fe lattice parameter (2.8544 Å). The mixing as well as the migration energies were determined with supercells of 54 atoms and 125 k points. The comparison between the ab initio results for the properties expressed in Eqs. (16)–(20) and the data obtained with the pair interactions appears in Table 4. The results are comparable with respect to signs and tendencies except for the mixing and interface energies of the Fe–Mn system maybe because of the Mn peculiar magnetic structure. It was thus, in a first step, decided to modify the Mn–Mn and the Mn–Ni binding energies in order to agree more with experiments (these values were increased by 0.2 eV). More accurate calculations (taking into account the possibility of noncollinear spins) are under way.

Moreover, according to their model of precipitate growth kinetics, Golubov et al. [31,32] found that the kinetic binding energy for Cu $E^{k}_{\mathrm{b}}(2) = E^{(1)}_{\mathrm{b(Cu\text{–}Cu)}} - E^{(1)}_{\mathrm{b(V\text{–}Cu)}}$ should be about 0.05 eV so that small Cu clusters could dissociate thermally to form

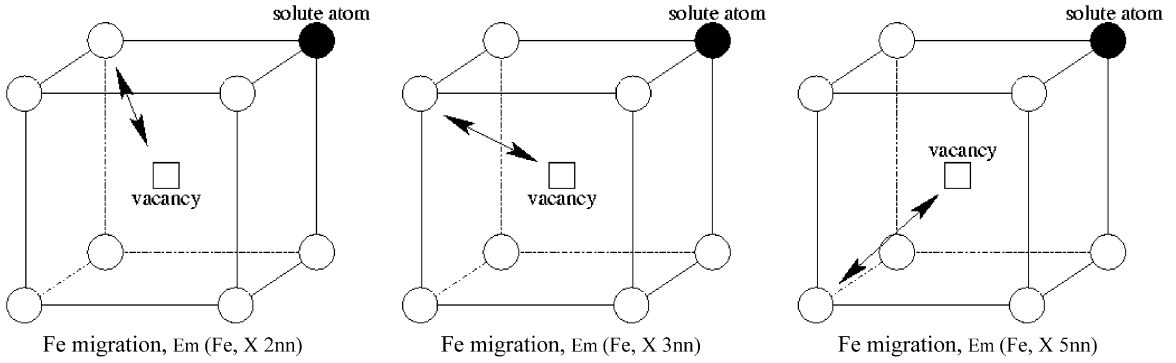

Fig. 1. Three different ways of migration for an iron atom with a solute atom in its vicinity. These three figures illustrate the migration energies presented in Tables 4 and 6.

Table 4
For each binary alloy Fe–X (X = Cu, Ni, Mn or Si), energies calculated from the properties used to parameterise the code compared to the corresponding energies obtained directly by ab initio calculations

Binary alloy	Fe–Cu		Fe–Ni		Fe–Mn		Fe–Si	
	Ab initio	Monte Carlo	Ab initio	Monte Carlo	Ab initio	Monte Carlo	Ab initio	Monte Carlo
E_{mix}(X = >Fe) (eV)	0.55	0.65	−0.12	−0.34	−0.10	−1.57	−1.07	−1.72
E_{int}(1 0 0) (mJ/m^2)	370	600	−385	−310	55	−1375	−2526	−1511
E_{int}(1 1 0) (mJ/m^2)	359	466	−298	−247	37	−1178	−1773	−1288
E_{mig}(Fe, X 2nn) (eV)	0.60	0.64	0.46	0.58	0.64	0.68	0.65	0.7
E_{mig}(Fe, X 3nn) (eV)	0.67	0.74	0.69	0.67	0.66	0.71	0.84	0.77
E_{mig}(Fe, X 5nn) (eV)	0.62	0.74	0.63	0.67	0.62	0.71	0.65	0.77

The mixing and migrating energies were calculated with 54 atom supercells and 125 k points. Barriers for different jumps of a Fe atom towards a vacancy were determined when a solute atom was in the vicinity of the migrating atom: E_m(Fe, X 2nn): the solute atom is second neighbour of the Fe atom before the jump, E_m(Fe, X 3nn): the solute atom is third neighbour, E_m(Fe, X 5nn): the solute atom is fifth neighbour of the Fe atom). Each jump is illustrated in Fig. 1.

bigger Cu clusters. The ab initio data were thus a bit modified to follow this model. Indeed, ab initio methods have limitations and the uncertainty of our calculations is close to 0.1 eV. The interface, mixing and migration energies obtained with the 'adjusted' data (Table 5) are collected in Table 6. Table 7 gathers the simulation parameters obtained with the new set of energies and Eqs. (6)–(15). We now present the results obtained with this set of parameters and compare them with experiments when appropriate.

Table 5
Modified binding energies (eV) compared to those determined previously by ab initio calculations

	Cu		Mn	
	Ab initio data	Adjusted data	Ab initio data	Adjusted data
E_b(X–X 1nn)			−0.28	−0.08
E_b(X–X 2nn)	0.03	0.09	−0.15	0.05
E_b(V–X 1nn)	0.17	0.11		
E_b(V–X 2nn)	0.19	0.09		
E_b(Ni–X 2nn)			−0.06	0.14
E_b(Ni–X 2nn)			−0.11	0.09

Table 6
New comparison of the mixing, interface, migration energies for the binary alloys Fe–X (X = Cu, Ni, Mn and Si)

	Fe–Cu		Fe–Ni		Fe–Mn		Fe–Si	
	Ab initio	Monte Carlo	Ab initio	Monte Carlo	Ab initio	Monte Carlo	Ab initio	Monte Carlo
E_{mix}(X= > Fe) (eV)	0.55	0.83	−0.12	−0.34	−0.10	−0.17	−1.07	−1.72
E_{int}(1 0 0) (mJ/m^2)	370	717	−385	−310	55	−213	−2526	−1511
E_{int}(1 1 0) (mJ/m^2)	359	630	−298	−247	37	−82	−1773	−1288
E_{mig}(Fe, X 2nn) (eV)	0.60	0.66	0.46	0.58	0.64	0.68	0.65	0.70
E_{mig}(Fe, X 3nn) (eV)	0.67	0.71	0.69	0.67	0.66	0.71	0.84	0.77
E_{mig}(Fe, X 5nn) (eV)	0.62	0.71	0.63	0.67	0.62	0.71	0.65	0.77

The new values calculated from Eqs. (16)–(20) have been obtained with the modified binding energies of Table 5.

Table 7
Pair interactions (eV) obtained from Eqs. (6)–(15) and from the final parameterisation energies

$\varepsilon^{(1)}_{(Fe–Fe)}$	−0.778	$\varepsilon^{(2)}_{(Si–Si)}$	−0.389	$\varepsilon^{(1)}_{(V–Cu)}$	−0.103	$\varepsilon^{(1)}_{(Cu–Mn)}$	−0.519
$\varepsilon^{(2)}_{(Fe–Fe)}$	−0.389	$\varepsilon^{(1)}_{(Fe–V)}$	−0.161	$\varepsilon^{(2)}_{(V–Cu)}$	−0.206	$\varepsilon^{(2)}_{(Cu–Mn)}$	−0.249
$\varepsilon^{(1)}_{(V–V)}$	0.315	$\varepsilon^{(2)}_{(Fe–V)}$	−0.161	$\varepsilon^{(1)}_{(V–Ni)}$	−0.234	$\varepsilon^{(1)}_{(Cu–Si)}$	−0.783
$\varepsilon^{(2)}_{(V–V)}$	−0.214	$\varepsilon^{(1)}_{(Fe–Cu)}$	−0.609	$\varepsilon^{(2)}_{(V–Ni)}$	−0.351	$\varepsilon^{(2)}_{(Cu–Si)}$	−0.374
$\varepsilon^{(1)}_{(Cu–Cu)}$	−0.581	$\varepsilon^{(2)}_{(Fe–Cu)}$	−0.344	$\varepsilon^{(1)}_{(V–Mn)}$	−0.151	$\varepsilon^{(1)}_{(Ni–Mn)}$	−0.831
$\varepsilon^{(2)}_{(Cu–Cu)}$	−0.389	$\varepsilon^{(1)}_{(Fe–Ni)}$	−0.821	$\varepsilon^{(2)}_{(V–Mn)}$	−0.206	$\varepsilon^{(2)}_{(Ni–Mn)}$	−0.464
$\varepsilon^{(1)}_{(Ni–Ni)}$	−0.793	$\varepsilon^{(2)}_{(Fe–Ni)}$	−0.399	$\varepsilon^{(1)}_{(V–Si)}$	−0.525	$\varepsilon^{(1)}_{(Ni–Si)}$	−0.974
$\varepsilon^{(2)}_{(Ni–Ni)}$	−0.389	$\varepsilon^{(1)}_{(Fe–Mn)}$	−0.648	$\varepsilon^{(2)}_{(V–Si)}$	−0.381	$\varepsilon^{(2)}_{(Ni–Si)}$	−0.369
$\varepsilon^{(1)}_{(Mn–Mn)}$	−0.438	$\varepsilon^{(2)}_{(Fe–Mn)}$	−0.364	$\varepsilon^{(1)}_{(Cu–Ni)}$	−0.692	$\varepsilon^{(1)}_{(Mn–Si)}$	−0.782
$\varepsilon^{(2)}_{(Mn–Mn)}$	−0.389	$\varepsilon^{(1)}_{(Fe–Si)}$	−0.902	$\varepsilon^{(2)}_{(Cu–Ni)}$	−0.344	$\varepsilon^{(2)}_{(Mn–Si)}$	−0.114
$\varepsilon^{(1)}_{(Si–Si)}$	−0.716	$\varepsilon^{(2)}_{(Fe–Si)}$	−0.469				

The constant α has been taken equal to 0.5, β to 1 as well as the constants λ for all solutes.

3. Results and discussion

3.1. Thermal ageing of binary alloys

First, a study of the thermal ageing at 300 °C of binary alloys Fe–X (X = Cu, Ni, Mn and Si) is presented. For each simulation, a bcc lattice of 40 unit cells in each of the three space directions with periodic boundary conditions was used. Within this matrix, 1.5 at.% of solute atoms and one single vacancy were introduced. At the beginning of the simulation, the 1920 solute atoms were randomly distributed among the 128 000 atoms and this random distribution led to the formation of a few small clusters (about a hundred doublets and less than ten triplets) for each kind of solute. The vacancy concentration (one vacancy for 128 000 atoms (8×10^{-6})) is very large compared to the experimental equilibrium vacancy concentration. The simulation time was thus rescaled as follows in order to obtain a physical time scale:

$$t = \left(\frac{C_{\mathrm{V,sim}}}{C_{\mathrm{v,real}}}\right) t_{\mathrm{MC}} \tag{21}$$

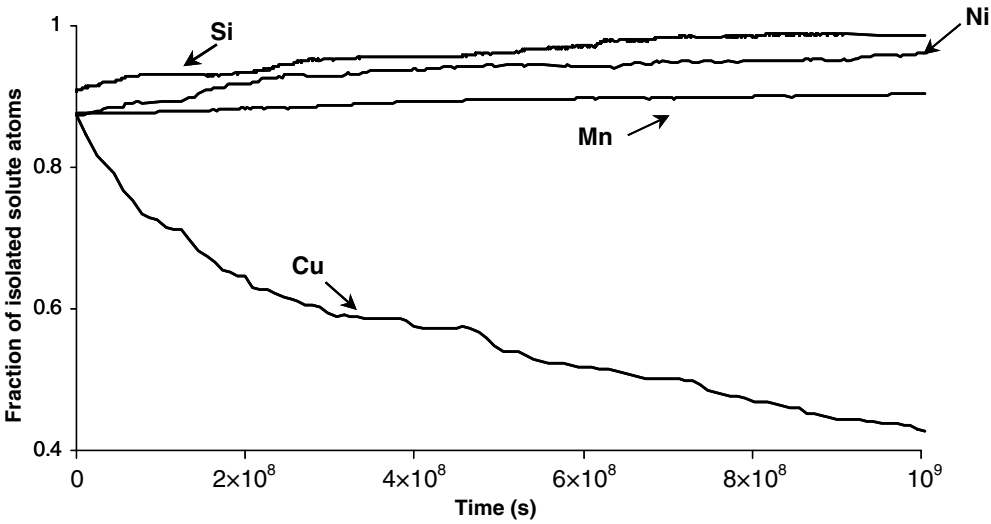

Fig. 2. Evolution of the number of isolated solute atoms as function of time. The time has been rescaled using Eqs. (21) and (22).

with

$$C_{v,real} = \exp\left(-\frac{E_{for}(V^{Fe})}{kT}\right)\exp\left(\frac{\Delta S}{k}\right) \times \left[1 - 8x_X - 6x_X + 8x_X \exp\left(\frac{E^{(1)}_{b(V-X)}}{kT}\right) + 6x_X \exp\left(\frac{E^{(2)}_{b(V-X)}}{kT}\right)\right]. \quad (22)$$

The equation giving $C_{v,real}$ takes into account the solute X concentration, x_X, and the vacancy–solute binding energies in order to obtain, from the vacancy formation energy in pure Fe, the value of the vacancy formation energy in the Fe–X binary alloy. $\frac{\Delta S}{k}$ equals 2 after the work of Mathon on the Fe–Cu system [33].

The evolution of the solute atoms distribution was followed during the simulation of each binary alloy and the fraction of isolated solute atoms as a function of the rescaled time t is reported in Fig. 2. The general behaviour of each solute is coherent with the binary phase diagrams and with the solution enthalpies that were determined by ab initio calculations [11]. First, it is clear that Cu behaves differently than the other solutes since it is the only one which precipitates all along the simulation.

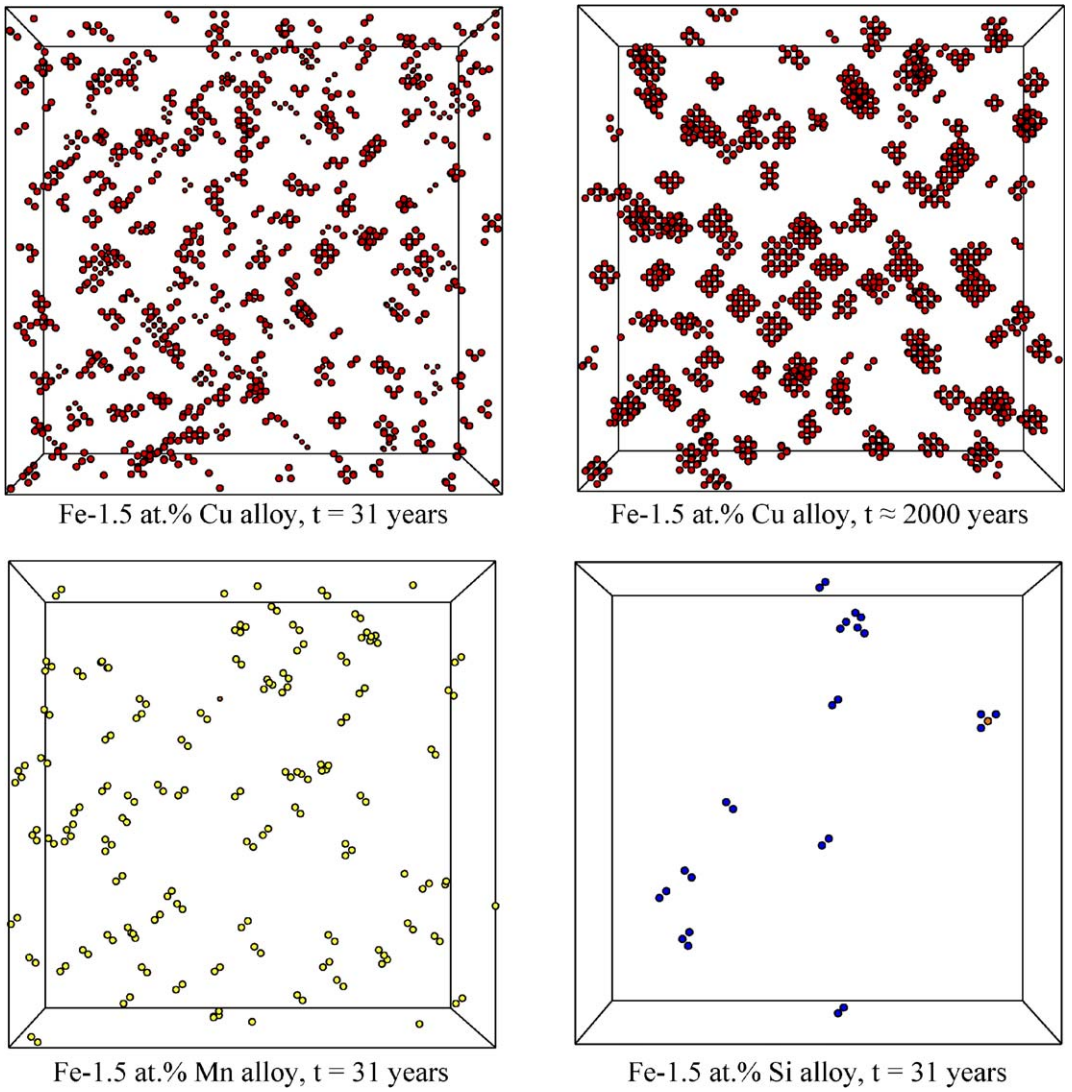

Fig. 3. Solute clusters distribution after about 31 years of thermal ageing at 573 K for the Fe–Cu, Fe–Mn and Fe–Si alloys. The vacancy is the orange circle and only the solute atoms which belong to a cluster are represented. Fe–1.5 at.%Cu alloy, $t = 31$ years Fe–1.5 at.%Cu alloy, $t \approx 2000$ years Fe–1.5 at.%Mn alloy, $t = 31$ years Fe–1.5 at.%Si alloy, $t = 31$ years. (For interpretation of the references in color in this figure legend, the reader is referred to the web version of this article.)

The Cu cluster distributions at two different times of the simulation appear in Fig. 3. After about 10^9 s or 31 years (rescaled time) of thermal ageing, clusters of a few atoms are formed (the larger cluster size is 17 atoms); and by continuing the simulation to longer times, these clusters grow (the bigger cluster is composed of 46 atoms). They are pure 3D Cu precipitates which are nonspherical with abrupt and quasi planar interfaces with the matrix. On the other hand, among Ni, Mn and Si atoms, Si dissolves the most: after 6×10^6 s or 70 days (rescaled time), 91% of the Si atoms are in the solid solution, and at the end of the simulation, 99% are in solution, as can be seen in Fig. 2. Fig. 3 shows that a few pairs and one triplet of Si atoms remain formed at the end of the simulation. The behaviour of the Fe–Ni alloy is similar to that of the Fe–Si one but the rate of Ni atoms within clusters is always higher, as can be seen in Fig. 2. In the Fe–Mn system, just a few Mn atoms diffuse very progressively in the solid solution. After 31 years of thermal ageing, the microstructure, which is illustrated in Fig. 3, is composed of many pairs and a few triplets of Mn atoms.

In a second step, a series of thermal ageing simulations have been performed between 663 and 773 K for a binary Fe–1.34 at.%Cu alloy. A rigid bcc lattice of 40 unit cells in each of the three space directions with periodic boundary conditions was used also. The Monte Carlo time has been rescaled using Eqs. (21) and (22). The precipitation advancement factor has been calculated during the simulations. It is given by

$$\zeta(t) = \frac{C_X(0) - C_X(t)}{C_X(0) - C_X(\infty)} \tag{23}$$

where $C_X(t)$ is the solute atom X concentration in the solid solution at time t, which tends towards the solubility limit $C_X(\infty)$. The precipitation kinetics predicted by our model are compared to the experimental results obtained by electrical resistivity measurements [34] in Fig. 4. For each temperature, two sets of results are presented in which the cluster

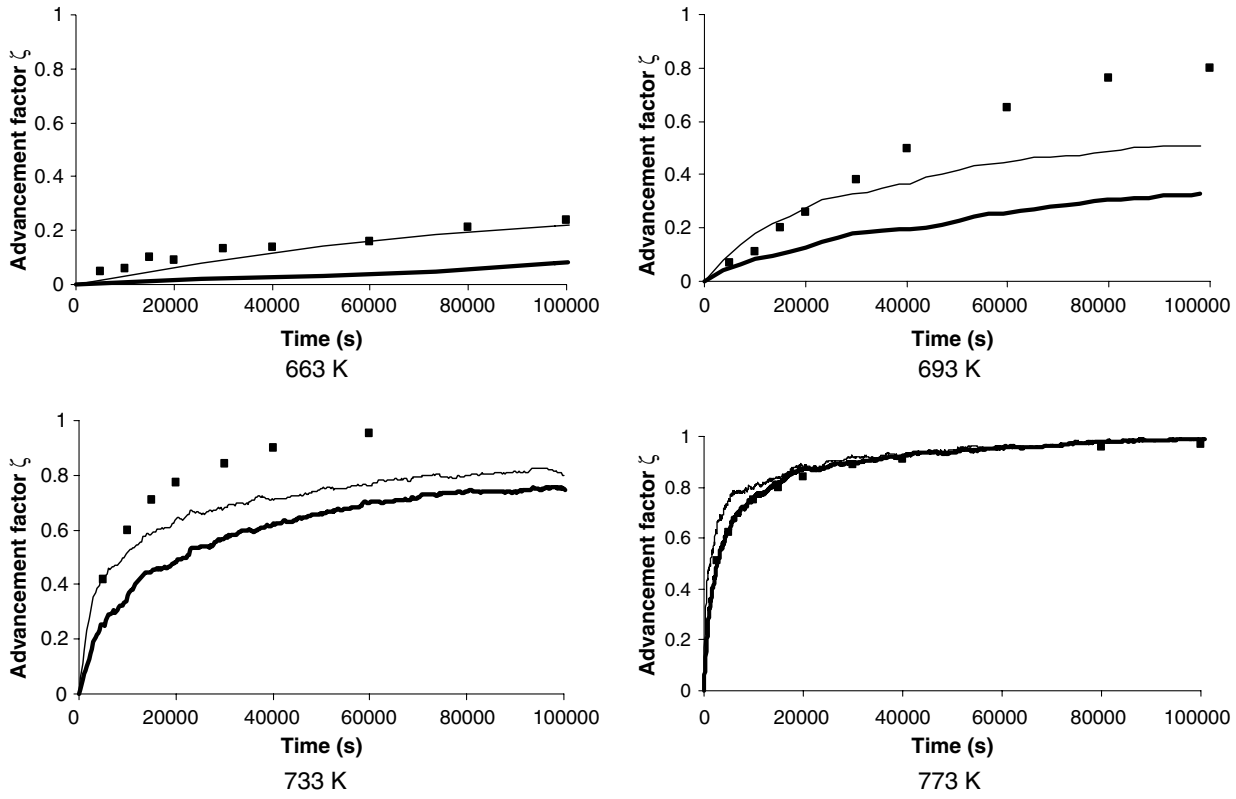

Fig. 4. Precipitation evolution of thermally aged Fe–1.34 at.%Cu alloys. The dots correspond to the experimental results of Lê et al. [34] and the curves to the Kinetic Monte Carlo results. The thin curve corresponds to the results obtained when only isolated Cu atoms are considered to be part of the solid solution while the thick curve corresponds to results obtained considering that clusters containing two or three Cu atoms also belong to the solid solution. The Kinetic Monte Carlo time was rescaled using Eqs. (21) and (22).

minimum size for a cluster to be considered as a cluster (and not part of the solid solution) differs. Indeed, for the set of results indicated by the thin curve, only isolated solute atoms were considered to be part of the solid solution whereas for the other one (thick curve), small clusters of 2 or 3 solute atoms were taken into account in the solid solution. The results appear in Fig. 4 for temperatures ranging from 663 to 773 K. The precipitation kinetics predictions of our model reproduce globally well the experimental result tendencies. The results obtained with the hypothesis that only isolated Cu atoms are part of the solid solution seem to be in better agreement with the experimental ones for the temperatures below 773 K whereas at 773 K, the two hypothesis lead to almost equivalent results.

3.2. Thermal ageing of a Fe–CuNiMnSi alloy

Simulations of thermal ageing of a Fe–0.2Cu0.63Si1.26Mn0.53Ni (in at.%) were performed

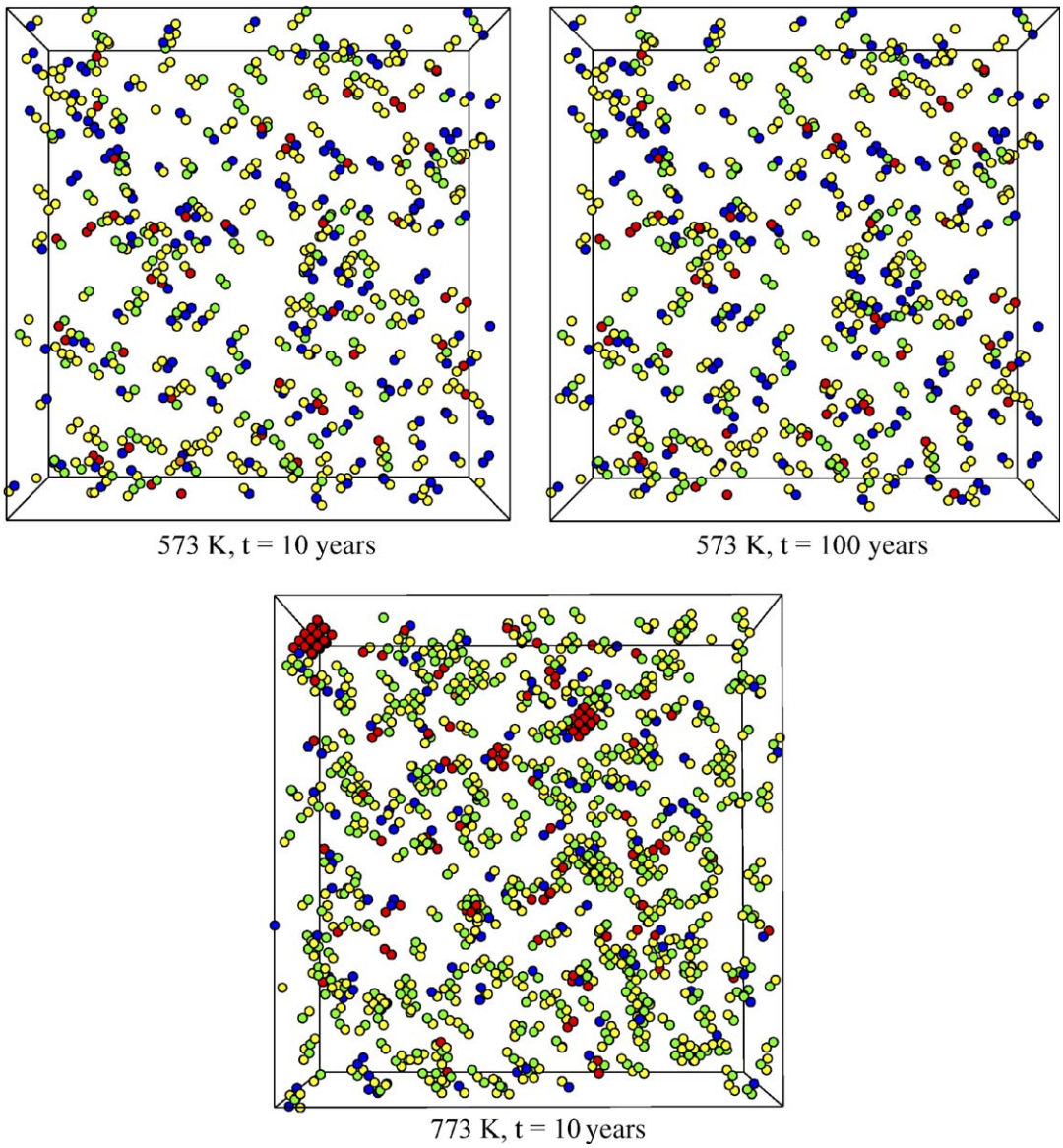

Fig. 5. Cluster distributions after thermal ageing of a Fe–0.2Cu0.63Si1.26Mn0.53Ni (at.%) at 573 and 773 K. The vacancy is black, the Cu atoms appear in red, the Mn ones in yellow, the Si ones in blue and the Ni atoms are green. Only the solute atoms belonging to a cluster are represented. (For interpretation of the references in color in this figure legend, the reader is referred to the web version of this article.)

at 573 and 773 K. A rigid bcc lattice of 40 unit cells in each of the three space directions with periodic boundary conditions was used also. The time was rescaled using Eq. (21) only. Fig. 5 displays the microstructural evolution results of this Fe–CuNiMnSi alloy after thermal ageing at these two temperatures. In the following, the study is made qualitatively on the cluster distribution size and composition. At 573 K, after 10 years of thermal ageing, clusters with a few Cu, Ni, Mn and/or Si solute atoms are formed. The bigger one is a 5-atom cluster with two Si atoms and 3 Mn atoms. By continuing the simulation until 100 years, the microstructure does not change so much. The three biggest clusters are each composed of five solute atoms. The first one contains two Si, one Mn and two Ni atoms as well as a vacancy; the second one is composed of one Si, three Mn and one Ni atoms and the last one of two Si and three Mn atoms. The fact that no Cu atoms are within the bigger clusters could be surprising (some are within the smaller ones (Fig. 5)), but this may indicate that a synergetic effect between all the solute atoms have an influence on their gathering. At 773 K, the microstructural aspect after 10 years of thermal ageing is radically different than the one obtained at 573 K for the same and even for the longest time since, at 773 K, precipitation has occurred (Fig. 5). Indeed, small Mn–Ni precipitates are formed as well as bigger ones with a Cu rich core surrounded by some Ni, Mn and/or Si atoms. The Mn–Ni precipitates are ordered and the bigger one contains eight Ni and eight Mn atoms. The two precipitates with a Cu rich core are composed respectively of 28 Cu, two Si and one Ni atoms and of 30 Cu, one Si, two Mn and two Ni atoms. A pure Cu precipitate of ten atoms is also formed. The formation of the precipitates which contain a pure Cu core surrounded by Ni, Mn and/or Si atoms is coherent with the thermodynamic data, as was explained by Liu et al. [8] to validate their results of Lattice Monte Carlo simulations of irradiated Fe–CuNiMn alloys. Indeed, since Mn, Ni and Si solute atoms have lower interface energies with the Fe atoms than the Cu atoms and since Mn, Ni and Si interact weakly with Cu (in first neighbour position), a Cu–Mn(Ni)(Si)–Fe transition interface produces a lower free energy than a Cu–Fe interface.

Modelling the formation of the solute clusters in a multi-component alloy is not an easy task. One has to take into account both the solute chemistry and the point defects. The simple approach by Liu et al. [8] and Odette and Wirth [9] provided important insights on the structure and composition of the nanometer clusters. In our model the final configurations (for almost infinite times) are very similar to those of Liu et al. [8] and Odette and Wirth [9] while bringing new information such as the kinetics of the formation of the clusters and the role of the point defects. In addition, the model of Liu et al. [8] and Odette and Wirth [9] is based on thermodynamical data and a few adjusted values, while our choice is to use ab initio data, which also had, for a few of them, to be adjusted.

Indeed, despite their predictive capabilities and the fact that they are at the moment the most precise methods at the atomic level, ab initio calculations have limitations. In our case, for instance, the energies we determine are very small and sometimes close to the uncertainty of the calculations. Furthermore, the influence of the collinearity of the spins imposed in our calculations has to be investigated in the case of Mn. Using ab initio data is not always straightforward and there is still a long way before multi-scale modelling of the evolution of the microstructure without using adjustable parameters. However the results obtained with this first set of parameters are very encouraging and should be suitable for the study of radiation damage and more specifically for the formation under neutron irradiation of the solute clusters in multi-component alloys.

4. Conclusion

We have run ab initio calculations related to the interactions between point defects and solute atoms in bcc Fe–X alloys (X = Cu, Ni, Mn and Si). The data have been used to parameterise an Atomic Kinetic Monte Carlo model to treat multi-component Fe–CuNiMnSi alloys. To validate the model, simulations of thermal ageing in different conditions of composition and temperature have been performed. The thermal ageing simulations of binary alloys are consistent with the experimental data. Indeed, with a concentration of 1.5 at.% of solute atoms in the matrix, the Cu is the only element which precipitates. Moreover, the temperature effect on the precipitation kinetics of a Fe–Cu alloy is fairly well reproduced, as compared to electrical resistivity results.

The kinetic Monte Carlo simulations of complex alloys agree qualitatively with the thermodynamic data since clusters that contain a pure Cu region

surrounded by a few Ni, Mn and/or Si solute atoms are formed. A temperature effect exists also on the evolution of these complex alloys.

A refinement of the parameterisation and a more quantitative study have now to be performed on thermally aged but also irradiated Fe–CuNiMnSi alloys.

Acknowledgements

This work has been performed within the European PERFECT project (FI6O-CT-2003-508840) which has sponsored this study. This research has been done using the CRI supercomputer of the USTL supported by the Fonds Européens de Développement Régional, as well as the CEA CCRT supercomputers in the framework of an EDF-CEA contract.

References

[1] M.K. Miller, B.D. Wirth, G.R. Odette, Mater. Sci. Eng. A 353 (2003) 133.
[2] J.T. Buswell, W.J. Phythian, R.J. McElroy, S. Dumbill, P.H.N. Ray, J. Mace, R.N. Sinclair, J. Nucl. Mater. 225 (1995) 196.
[3] B.D. Wirth, PhD Dissertation, University of California, Santa Barbara, 1995.
[4] P. Auger, P. Pareige, M. Akamatsu, J.C. Van Duysen, J. Nucl. Mater. 211 (1994) 194.
[5] B. Radiguet, PhD thesis, Université de Rouen, 2004.
[6] M.K. Miller, P. Pareige, Mater. Res. Soc. Symp. 650 (2001) R6.1.1.
[7] M.K. Miller, M.G. Burke, J. Nucl. Mater. 195 (1992) 68.
[8] C.L. Liu, G.R. Odette, B.D. Wirth, G.E. Lucas, Mater. Sci. Eng. A 238 (1997) 202.
[9] G.R. Odette, B.D. Wirth, J. Nucl. Mater. 251 (1997) 157.
[10] A. Cerezo, S. Hirosawa, I. Rozdilsky, G.D.W. Smith, Philos. Trans. R. Soc. Lond. A 361 (2003) 463.
[11] E. Vincent, C.S. Becquart, C. Domain, Nucl. Instrum. and Meth. B 228 (2005) 137.
[12] G. Kresse, J. Hafner, Phys. Rev. B 47 (1993) 558; G. Kresse, J. Hafner, Phys. Rev. B 49 (1994) 14251.
[13] G. Kresse, J. Furthmüller, Comput. Mater. Sci. 6 (1996) 15.
[14] C. Domain, C.S. Becquart, Phys. Rev. B 65 (2002) 024103.
[15] C. Domain, C.S. Becquart, J.C. Van Duysen, Mater. Res. Soc. Symp. Proc. 650 (2001) R3.25.1.
[16] W.M. Young, E.W. Elcock, Proc. Phys. Soc. 89 (1966) 735.
[17] F. Soisson, A. Barbu, G. Martin, Acta Mater. 44 (1996) 3789.
[18] F. Soisson, G. Martin, Phys. Rev. B 62 (2000) 203.
[19] C. Domain, C.S. Becquart, J.C. Van Duysen, Mater. Res. Soc. Symp. Proc. 540 (1999) 643.
[20] F. Soisson, Y. Le Bouar, Phys. Rev. B 65 (2002) 094103.
[21] S. Schmauder, P. Binkele, Comput. Mater. Sci. 24 (2002) 42.
[22] V. Raghavan, J. Phase Equilib. 23 (2002) 267.
[23] M. Hasebe, T. Nishizawa, Applications of Phase diagrams in metallurgy and ceramics, vol. 2, NBS Special Publication 496 (1978) 910, Washington DC, National Bureau of Standards.
[24] F.M. Wang, X.P. Li, Q.Y. Han, N.X. Zhang, Metall. Mater. Trans. B 28B (1997) 109.
[25] P. Fan, K.C. Chou, Metall. Mater.Trans. A 30A (1999) 3099.
[26] K.J. Rönkä, A.A. Kodentsov, P.J.J. Van Loon, J.K. Kivilahti, F.J.J. Van Loo, Metall. Mater. Trans. A 27A (1996) 2229.
[27] H. Li, A. Morris, Metall. Mater. Trans. B 8B (1997) 553.
[28] H. Ohta, H. Suito, ISIJ Int. 43 (2003) 1301.
[29] D. Hobbs, J. Hafner, D. Spišák, Phys. Rev. B 68 (2003) 014407.
[30] C. Kittel, Introduction to Solid State Physics, 6th Ed., Wiley, New York, 1987.
[31] S.I. Golubov, Yu.N. Osetsky, A. Serra, A.V. Barashev, J. Nucl. Mater. 226 (1995) 252.
[32] Yu.N. Osetsky, A. Serra, Philos. Mag. A 73 (1) (1996) 249.
[33] M.H. Mathon, PhD thesis, Université d'Orsay, Paris-Sud, 1995.
[34] T.N. Lê, A. Barbu, D. Liu, F. Maury, Scr. Metall. Mater. 26 (1992) 771.
[35] A. Möslang, E. Albert, E. Recknagel, A. Weidinger, P. Moser, Hyperfine Interact. 15/16 (1983) 409.
[36] G. Brauer, K. Popp, Phys. Status Solidi B 102 (1987) 79.
[37] H.E. Schaefer, K. Maier, M. Weller, D. Herlach, A. Seeger, J. Diehl, Scr. Metall. 11 (1977) 803.
[38] L. De Schepper, D. Segers, L. Dorikens-Vanpraet, M. Dorikens, G. Knuyt, L.M. Stals, P. Moser, Phys. Rev. B 27 (1983) 5257.